Island Cells Control Temporal Association Memory

Citation: Kitamura, T., M. Pignatelli, J. Suh, K. Kohara, A. Yoshiki, K. Abe, and S. Tonegawa. "Island Cells Control Temporal Association Memory." Science 343, no. 6173 (February 21, 2014): 896–901.

As Published: http://dx.doi.org/10.1126/science.1244634

Publisher: American Association for the Advancement of Science (AAAS)

Persistent URL: http://hdl.handle.net/1721.1/85965

Version: Author's final manuscript: final author's manuscript post peer review, without publisher's formatting or copy editing

Island Cells Control Temporal Association Memory

Takashi Kitamura[1]*, Michele Pignatelli[1]*, Junghyup Suh[1], Keigo Kohara[1],

Atsushi Yoshiki[2], Kuniya Abe[2] and Susumu Tonegawa[1, 3]†

[1]RIKEN-MIT Center for Neural Circuit Genetics at the Picower Institute for Learning and Memory, Department of Biology and Department of Brain and Cognitive Sciences, Massachusetts Institute of Technology, Cambridge, MA 02139, U.S.A.

[2]RIKEN BioResource Center, 3-1-1 Koyadai, Ibaraki 305-0074, Japan

[3]Howard Hughes Medical Institute at MIT, Cambridge, MA 02139, U.S.A.

*These authors contributed equally to this work.

†To whom correspondence should be addressed: tonegawa@mit.edu

One Sentence Summary:

We found a distinct set of excitatory neurons (Island cells), which appear in a curvilinear matrix of bulb-like structures in layer II of the entorhinal cortex, project directly to pyramidal cell dendrite-targeting inhibitory neurons in the hippocampal CA1 area, and control the formation of temporal association memory driven by layer III of the medial entorhinal cortex.

Episodic memory requires associations of temporally discontiguous events. In the entorhinal-hippocampal network, temporal associations are driven by a direct pathway from layer III of the medial entorhinal cortex (MECIII) to the hippocampal CA1 region. However, the identification of neural circuits that regulate this association has remained unknown. In layer II of entorhinal cortex (ECII) we report clusters of excitatory neurons called Island Cells, which appear in a curvilinear matrix of bulb-like structures, directly project to CA1 and activate interneurons that target the distal dendrites of CA1 pyramidal neurons. Island Cells suppress the excitatory MECIII input through the feedforward inhibition to control the strength and duration of temporal association in trace fear memory. Together, the two EC inputs comprise a control circuit for temporal association memory.

Word Count125/125

Word Count 4,245/ 2,500 (report)

Episodic memory consists of associations of objects, space and time (*1*). In humans and animals, the entorhinal cortex (EC)-hippocampal (HPC) network plays an essential role in episodic memory (*2*), with medial EC (MEC) and lateral EC (LEC) inputs into HPC providing spatial and object information, respectively (*3*). Neural circuits have been identified in the EC-HPC network that mediate space and object associations (*4-6*). In contrast, the neural circuits for time-related aspects of episodic memory are only beginning to be studied (*7, 8*). Direct inputs from MEC layer III cells to CA1 pyramidal cells drive the temporal association of discontiguous events (*9*). Like most cognitive and motor phenomena temporal association memory must be regulated for optimal adaptive benefit, yet virtually nothing is known about the underlying mechanisms of this regulation. Here, we investigated this issue by mapping and characterizing an unsuspected neuronal circuit within the EC-HPC network and examining the effect of its optogenetic manipulations on a temporal association memory.

A retrograde tracer, cholera toxin subunit B (CTB), was injected into the DG of C57BL6 mice (Fig. 1A). While a majority of cells in ECII were CTB-positive, a large proportion was CTB-negative and clustered in a series of about 130 μm diameter bulb-like structures (Fig. 1B-C). Hereafter, we refer to these CTB-negative cells as ECII Island (ECIIi) cells. ECIIi cells are mostly pyramidal (Fig. 1F, fig. S1) and express Wfs1 (*10*) and CalbindinD-28K (*11*) (Fig. 1B-D, F). CTB-positive cells were identified as previously well known DG-projecting stellate cells (*12, 13*) (Fig. 1G, fig. S1-2) that express Reelin (*14*) but not Wfs1 or CalbindinD-28K (Fig. 1E). Hereafter, we refer to these CTB-positive cells as ECII Ocean (ECIIo) cells. ECIIi cells are excitatory (Fig. 1F, fig. S1-2) and present in both MEC and LEC (fig. S2), but are distinct from ECIIo cells not only by their morphology and molecular markers but also by their intrinsic electrophysiological properties (*15, 16*) (fig. S1).

We created a Cre transgenic mouse line using the Wfs1 promoter (fig. S3). When the Cre-dependent virus AAV_9-EF1α-DIO-eYFP was injected into the superficial layers of the EC (Fig. 1H), eYFP expression was restricted to Wfs1- and CalbindinD-28K-positive ECIIi cells (Fig. 1I-J, fig. S4). These ECIIi cells appeared in a curvilinear matrix of bulb-like structures in tangential MEC sections (Fig. 1K). We injected the AAV_9-EF1α-DIO-ChR2-eYFP virus (*17*) into the EC of Wfs1-Cre mice (Fig. 1L). ECIIi cells projected primarily to the CA1 region via the temporoammonic pathway (Fig. 1M). Additional weaker projections were detected in the subiculum, parasubiculum, contralateral CA1 and EC (Fig. 1M, fig. S5). Wfs1- and CalbindinD-28K-positive ECIIi cells are also present in rat and project to the CA1 region (fig. S6).

In the CA1 region, ECIIi axons specifically innervated the border between the stratum-radiatum (SR) and stratum-lacunosum-moleculare (SLM) (Fig. 2A), terminating sharply at the proximal end of CA1, and did not enter into CA2 (Fig. 2A) that was marked with RGS14 (*18*). ECIIi axons were strongly myelinated (fig. S7) (*19*) and preferentially innervate the stratum-lacunosum (SL) (Fig. 2B). In contrast, MECIII axons innervate the stratum-moleculare (SM) immediately

adjacent to the SL (Fig. 2C). Experiments conducted with VGAT-promoter-ChR2eYFP transgenic mice (*20*) and anti-GAD67 suggested that the primary target of the ECIIi cells are GABAergic interneurons in the SL (SL-INs) (Fig. 2D-F) (*21*). Presynaptic terminal analysis showed ECIIi cells are glutamatergic (Fig. 2G, fig. S8). Low expression of PSD-95 in the SL suggested that innervations of ECIIi axons onto CA1 pyramidal cell dendrites in the SL are relatively infrequent (fig. S9).

Optogenetic stimulation of ChR2-expressing ECIIi axons during *in vitro* patch-clamp recordings of SL-INs revealed reliable excitatory postsynaptic currents (EPSCs, average amplitude 54 ± 7 pA, average onset 2.05 ± 0.07 ms, n = 40) in 87% of SL-INs (n = 53, Fig. 2H-J, fig. S10), which were sensitive to ionotropic glutamate receptor antagonists (fig. S11). In current mode, repetitive photostimulation was sufficient to trigger action potentials in SL-INs (n = 14 out of 40, Fig. 2K and Q). Under similar stimulation conditions CA1 pyramidal cells showed small EPSCs (average amplitude 19 ± 5 pA, average onset 3.11 ± 0.08 ms, n = 29) in 70% of them (n = 50, Fig. 2L-N, fig. S11), suggesting a weaker impact of ECIIi cells to CA1 pyramidal cells than to SL-INs (Fig. 2P). In current mode, repetitive photostimulation never triggered action potentials in CA1 pyramidal cells (n = 35). However, somatic depolarization to -55 mV revealed strong inhibitory potentials (IPSPs) in 30% of CA1 pyramidal cells (n = 50, Fig. 2O) in response to optogenetic stimulation of ECIIi axons, which was abolished by bath application of GABA receptor antagonists (Fig. 2R). These data demonstrate a previously unknown feedforward inhibitory circuit controlled by ECIIi cells (Fig. 2S).

Input selectivity to SL-INs was investigated by replacing the Wfs1-Cre transgenic mice with the MECIII cell-specific pOxr1-Cre mice (*9*) or the CA3 cell-specific KA1-Cre transgenic mice (*5*) (Fig. 3A-C). SL-INs were preferentially innervated by ECIIi cells (Fig. 3D-G, see supplemental statistics).

The SL-INs exert an inhibitory effect on the apical dendrite of CA1 pyramidal cells (*22*). To investigate whether the ECIIi-SL-INs circuit has the ability to inhibit MECIII inputs to CA1 pyramidal cells, the AAV_9-EF1α-DIO-ChR2-eYFP virus was injected into the EC of pOxr1-Cre mice. We then simultaneously recorded connected pairs of SL-INs and CA1 pyramidal cells (Fig. 3H) to test whether SL-INs activity was sufficient to inhibit MECIII input. We found 8 connected pairs out of 260 tested pairs ($P_{connection}$ = 0.03, average uIPSP amplitude -0.18 ± 0.09 mV, average uIPSP onset 1.45 ± 0.2 ms, Fig. 3I). Confocal microscopic analysis suggested an average of 2 ± 0.3 putative synaptic contacts between SL-INs axons and CA1 pyramidal cell's apical dendrites (inset, Fig. 3H, fig. S12). By eliciting a brief burst in SL-INs we observed IPSPs in all the connected CA1 pyramidal cells (Fig. 3J). Optogenetic stimulation of MECIII axons elicited EPSPs in CA1 pyramidal cells (Fig. 3K). However, pairing optogenetic stimulation and SL-IN stimulation significantly reduced the amplitude of EPSP to 60% of the response evoked by MECIII axonal stimulation alone (average amplitude: MEC-stimulation only 1.6 ± 0.4 mV, pairing MEC/SL-INs 0.9 ± 0.4 mV n = 8, Fig. 3K-L). The lack of significant difference between

the average IPSP amplitude and the inhibited component of the response suggested a reduction mediated mainly by linear subtraction (Wilcoxon signed-rank P = 0.5).

We then sought the functional significance of ECIIi-SL-IN circuit-mediated inhibition of MECIII input to CA1 at the behavioral level. For this purpose, we injected bilaterally AAV_9-CBA-DIO-ArchT-eGFP (*23*) into the EC of pOxr1-Cre mice. Unilateral shining of green light to a CA1 area of these mice with an optic fiber implanted to this area (*24*) (Fig 4A, fig. S13) inhibited the ArchT-expressing MECIII axons resulting in a reduction of the multiunit activity of CA1 pyramidal cells *in vivo* (58% reduction, Fig. 4B). We subjected mice to trace fear conditioning (TFC) while delivering green light bilaterally to the CA1 areas during the entire training period (i.e. 3 rounds of tone, trace and shock periods). Mice expressing ArchT, but not control mice expressing the fluorescence marker only (i.e. tdTomato), exhibited severe freezing deficits during both training and testing sessions (Fig. 4C-D) but not in response to the context (fig. S15). The remaining freezing observed during the tone period of the testing session is likely due to non-associative learning (fig. S14).

We injected bilaterally AAV_9-EF1α-DIO-ChR2-eYFP into the EC of Wfs1-Cre mice. Unilateral shining of blue light to a CA1 area resulted in reduced multiunit activity of CA1 pyramidal cells *in vivo* (46% reduction, Fig 4B), strongly supporting the feedforward inhibition of CA1 activity by the ECIIi-INs pathway, which was demonstrated also by the *in vitro* study (Fig. 2O). In TFC, these mice exhibited severe freezing deficits both during training (Fig. 4E) and testing (Fig. 4F) sessions compared to the three control groups when blue light pulses were delivered bilaterally to the CA1 areas during the entire training period. The freezing deficits were particularly large during the post-tone periods of the testing session. In contrast, the ChR2 light-ON group froze as much as the control groups in response to the training context (fig. S15). When light of the same intensity and duration was delivered to the ChR2 group prior to (82 s before) the training period, there was no light effect on freezing (fig. S16). The delivery of blue light pulses during the entire training period had no effect on freezing when mice were subjected to delayed fear conditioning (DFC) in which trace was omitted (Fig. 4G-H), indicating that deficits observed in TFC (Fig. 4E-F) are not due to an inability to encode the CS or US. A direct stimulation of SL-INs in VGAT-ChR2-eYFP transgenic mice by blue light during the training period caused freezing deficits in TFC but not in response to the context (fig. S17).

We restricted the stimulation to the trace plus footshock period (Tr-S group) or to the tone period (To group). The light-ON Tr-S group showed severe freezing deficits during both training and post-tone periods of testing sessions (Fig. 4I-J). The pattern of freezing deficits of the Light-ON Tr-S group and the light-ON ChR2 group were comparable during both training and testing sessions. The light-ON To group did not show any significant freezing deficits either during the training or testing session (Fig. 4I-J).

We subjected eArch3.0eYFP-expressing (eArch group) (*17*) and eYFP only-expressing (eYFP group) Wfs1-Cre mice to *in vivo* recordings. The stimulation of the eArch3.0-positive ECIIi

axons in the CA1 area with green light increased the multiunit activity of CA1 pyramidal cells (30% enhancement, Fig 4B). We subjected them to TFC with green light delivered bilaterally during the entire training period. During the training session, the eArch group showed as much freezing as the control eYFP group (Fig. 4K). However, during the testing session, the eArch group displayed significantly enhanced freezing during the post-tone periods that lasted about 1 min longer compared to the control eYFP group (Fig. 4L) but freezing was unaltered in response to the context (fig. S15). Maximal levels of freezing were unaltered during training and testing sessions, although this could be due to a ceiling effect of the training protocol. Indeed, when the strength of the footshocks was lowered, the maximal levels and the post-tone duration of freezing were greater in the eArch group compared to the control eYFP group during both training and testing sessions (Fig. 4M-N). We injected AAV_9-EF1α-DIO-ChR2-mCherry into the EC of pOxr1-Cre mice. The blue light pulse stimulation to the CA1 area increased the multiunit activity of CA1 pyramidal cells *in vivo* (31% enhancement, Fig 4B). We subjected ChR2mCherry-expressing (ChR2 group) and mCherry only-expressing (mCherry group) pOxr1-Cre mice to TFC with the lower shock intensity with blue light stimulations during the trace period. During the testing session, the ChR2 group displayed significantly enhanced freezing amplitudes and post-tone freezing duration compared to the control mCherry group (Fig. 4O-P).

The interplay of synaptic excitation and inhibition contributes to the regulation of perception, memory and motor behavior (*25*). A major challenge in neuroscience is to define this interplay at the levels of specific neuronal circuits and the specific cell types participating in them. We identified and characterized a neural circuit in the EC-HPC network that regulates temporal association memory, an essential component of episodic memory.

Previous studies have determined that approximately one-third of ECII excitatory cells are made of pyramidal cells (*15, 16, 26*), but their projections to SL-INs in CA1 has been unknown. The modularity of ECII neurons has been reported previously. The patch-like structures identified by anti-CalbindinD-28K (*11*) and "islets" detected by the expression of Wfs1 mRNA (*10*) probably correspond to our ECIIi's. However, projections of these subpopulations of ECII cells into HPC have not been reported previously. Cytochrome oxidase (CO) staining revealed patches of axonal terminals in ECII that are derived from metabolically active cells (*27, 28*). These CO-patched are larger than ECIIi's and contain both CalbindinD-28K-positive ECIIi cells (fig. S6) and stellate cells (*28*).

The strategic location of SL-INs, the primary target of ECIIi cells, immediately adjacent to the inner side of the SM layer where MECIII cells synapse to the distal dendrites of CA1 pyramidal cells enable ECIIi cells to suppress MECIII input by feedforward inhibition. Our findings are consistent with previous studies pointing to the existence of a feedforward inhibitory circuit arising from direct entorhinal inputs into CA1 (*29, 30*). However, these earlier studies utilized electrical stimulation of SLM axons and hence could not distinguish ECIII and ECIIi axons which run in the SM and SL, respectively. SL-INs are connected by gap junctions (*31*). Thus,

activation of ECIIi axons can evoke a depolarizing response broadly among SL-INs, which propagates through gap junctions amplifying the effect of ECIIi cell inputs.

Our behavioral data allow for two important conclusions. First, the fact that behavioral freezing in TFC was optogenetically impaired by either inhibition of MECIII input or activation of ECIIi input provides evidence for inhibition of the former input by the latter through feedforward inhibition. This conclusion is reinforced by the enhanced freezing level and the prolonged post-tone freezing period induced by eArch-mediated inactivation of the ECIIi axons. Thus, the freezing response can be regulated bidirectionally by the relative strength of MECIII and ECIIi inputs to CA1. Our data suggest that this regulatory system controls the strength of a temporal association memory as well as the duration of the expression of this memory after the recall cues cease. Such a regulation is crucial for optimal adaptive benefit; too strong an association of a particular pair of events may interfere with associations of other useful pairs while too weak an association for a given pair of events will not result in an effective memory. Perhaps even more importantly, the ECIIi-INs pathway input can provide a specific pattern of temporal windows within which MECIII input can drive the associations. While all the physiological and behavioral data support the binary regulation of the temporal association memory by the MECIII and ECIIi inputs, a future study focusing on *in vivo* recordings of the animals undergoing the task would be highly informative.

Second, our observation that the freezing deficit was caused by the inhibition of MECIII input by the ECIIi-CA1 pathway during the trace and shock period but not during the tone period indicates that the trace is not stored in CA1 and that post-tone MECIII input is crucial for the formation of temporal association memory. We propose that the source of this input could be persistent activity triggered in MECIII by the tone (*9, 32, 33*). Such activity will be transmitted to CA1 pyramidal cells, and then to the basolateral amygdala via the EC layer V (ECV) (*34*) as a CS (i.e. tone signal) coincident with the US (i.e. shock signal) to generate a fear memory engram via Hebbian synapses in the basolateral amygdala (*35*). The tone-triggered persistent activity in ECIII may also be instrumental for the prolonged post-tone freezing during recall of the temporal association memory.

Although our study has demonstrated that the feedforward inhibition of MECIII input to CA1 pyramidal cells by the ECIIi-SL-INs pathway serves as an important mechanism for the control of temporal association memory, other circuits and/or mechanisms may also contribute to this process. For instance, a recent study described long range projections of entorhinal interneurons into HPC interneurons including SL-INs (*36*). This circuit could also participate in the regulation of temporal association memory by countering the effect of the ECIIi-SL-INs circuit. Another possibility is that SL-INs may contribute to the regulation of temporal association memory by rhythmic dendritic inhibition of CA1 pyramidal cells through their rhythmic activation (*22*).

CA1 pyramidal cells receive a multitude of other excitatory and inhibitory inputs (*26*) including the Schaffer collateral (SC) input from CA3 that originates from ECIIo cells. While the *in vitro*

interaction of ECIII and CA3 inputs on the activity and synaptic plasticity of CA1 pyramidal cells have been reported (*37*), the inhibition of SC input does not seem to have a significant effect on the TFC performance (*9*). Although the role of the direct pathway, ECIIi-CA1 pyramidal cells, has not been yet elucidated, we hypothesize that the indirect pathway from ECIIo to CA1 via the trisynaptic circuit primarily processes context and space while the direct pathways from MECIII and ECIIi-SL-INs are responsible for temporal properties of episodic memory.

Fig. 1 Characterizations of Island Cells and generation of Wfs1-Cre transgenic mice

(A) Injection sites of CTB (red) in DG. **(B)** Parasagittal sections of MEC visualized with CTB-labeled cell bodies (red) and immunostained with anti–Wfs1 (green). Arrowheads: Wfs1-positive and CTB-negative ECIIi cells. **(C)** Magnified image from (B). **(D)** Parasagittal sections of EC immunostained with anti–Wfs1 (green) and anti-Calbindin D-28K (red). **(E)** Parasagittal sections of EC immunostained with anti–Wfs1 (green) and anti-Reelin (red). Wfs1-positive cells do not express the Reelin. **(F-G)** Examples of biocytin-stained Wfs1-positive pyramidal cell (F) and Reelin-positive stellate cell (G). Electrophysiological responses to positive or negative current step injections. **(H)** Transgenic mouse combined with AAV injection. **(I-J)** Parasagittal sections of Wfs1-Cre mouse injected with AAV_9-EF1α-DIO-eYFP (green) and immunostained with anti-Wfs1 (red) and anti-CalbindinD-28K (blue). **(K)** Tangential MEC sequential caudo-rostral sections of a Wfs1-Cre mouse injected with AAV_9-EF1α-DIO-eYFP. **(L-M)** Parasagittal sections of a Wfs1-Cre mouse injected with AAV_9-EF1α-DIO-ChR2-eYFP. Injection site (EC) (L). Hippocampal innervations (M). TA, temporoammonic pathway; PaS, parasubiculum; S, subiculum, D, dorsal; V, ventral; R, rostral; C, caudal; L, lateral; M, medial.

Fig. 2 Island Cells project to GABAergic neurons in the Stratum-Lacunosum layer of CA1

(A) Parasagittal HPC section of Wfs1-Cre mouse injected with AAV_9-EF1α-DIO-ChR2-eYFP (green) and immunostained with anti-RGS14 (red). **(B)** Magnification of the boxed area in (A). Stratum-lacunosum (SL) is a component of SLM. **(C)** Parasagittal section of MECIII-specific pOxr1-Cre mouse injected with AAV_9-EF1α-DIO-ChR2-eYFP (green) and immunostained with anti–Wfs1 (violet). Stratum-moleculare (SM) is a component of SLM. **(D-E)** Parasagittal sections of double transgenic mice, VGAT-ChR2-eYFP crossed with Wfs1-Cre (D), or with pOxr1-Cre (E) crossed injected with AAV_9-EF1α-DIO-ChR2-mCherry (red) into EC. **(F)** Parasagittal section of Wfs1-Cre mouse injected with AAV_9-EF1α-DIO-ChR2-mCherry (red) and immunostained by anti-GAD67 (green) and anti-NeuN (blue). Arrowheads: GAD67-positive neurons in the SL. **(G)** Parasagittal sections of Wfs1-Cre mouse injected with AAV_9-EF1α-DIO-Synaptophysin-mCherry (red) as a presynaptic terminal marker and immunostained with anti–VGLUT1 (green). Arrowheads indicate the VGULT1-positive presynaptic terminals of ECIIi cell axons. **(H and L)** Zeta-projected confocal image of biocytin-filled (violet) SL-IN (H) or CA1 pyramidal cell (L). ECIIi axons (green). **(I and M)** Optogenetic stimulation of ECIIi axons combined with patch-clamp recordings of SL-INs (I) or CA1 pyramidal cells (M). **(J and N)** EPSCs elicited in SL-IN (in H) or in CA1 pyramidal cells (in L) in response to optogenetic stimulation of ECIIi axons. **(K)** Optogenetic stimulation evoked action potential in the SL-IN recorded in current mode at resting membrane potential. **(O)** Feedforward inhibition in CA1 pyramidal cell recruited by optogenetic stimulation of ECIIi axons. **(P)** Kinetic of the EPSCs elicited by optogenetic stimulation of ECIIi axons. EPSCs recorded in SL-INs displayed larger

amplitude (KS<0.001) and faster onset (KS<0.001) than EPSCs recorded in pyramidal cells. **(Q)** SL-INs' average action potential (AP) probability in response to optogenetic stimulations of ECIIi axons. **(R)** Feedforward inhibition recruited in CA1 pyramidal cells is abolished by bath application of GABA receptor antagonists (Wilcoxon signed-rank P<0.05, n=7). See example in (O). **(S)** Schematic of the feedforward inhibition. Thickness of the lines indicates connection strength.

Fig. 3 Inhibition of ECIII input to CA1 by Island Cells through SL-GABAergic neurons

(A-C) Expression of ChR2-eYFP (green) in CA3-specific (A), ECIIi-specific (B) and MECIII specific (C) transgenic mice. SL-INs stained by biocytin (violet). Voltage clamp recording of light evoked EPSCs in SL-INs following optogenetic stimulation of CA3 (A), ECIIi (B) or MECIII (C) axons. **(D-G)** Connection probability (Fisher exact test **P<0.005, ***P<0.001, D), EPSC amplitude (Wilcoxon sum rank *P<0.05, ***P<0.001, E), EPSC onset (Wilcoxon sum rank **P<0.005, ***P<0.001, F), firing probability (Fisher exact test *P<0.05, G) in response to optogenetic stimulation of CA3, ECIIi or MECIII axons. **(H)** Zeta-projected confocal image of biocytin-filled SL-INs (IN1, IN2, IN3) and CA1 pyramidal cells (P1, P2). MECIII axons (green). Inset from the dotted-line box: putative contact points between IN2 and P1 (red asterisks). **(I)** Connectivity matrix of cells displayed in H. Only IN2-P1 showed IPSPs. **(J)** Schematic, raw traces and average amplitude (n=8 pairs) of the IPSPs evoked in P1 by stimulation of IN2. **(K)** Schematic, raw traces and average amplitude (n=8 pairs) of the EPSPs evoked in P1 by optogenetic stimulation of MECIII fibers. **(L)** Schematic and raw traces showing the response recorded in P1 to simultaneous stimulation of MECIII axons and IN2. Note the reduction elicited by the simultaneous stimulation when compared to optogenetic stimulation of MECIII axons only (Wilcoxon signed-rank *P<0.05, n=8 pairs, average in red).

Fig. 4 Effects of optogenetic axonal excitation and inhibition on behavior

(A) *in vivo* multiunit recording in anaesthetized mice combined with optogenetic axonal excitation or inhibition. **(B)** Upper panels: example of light-induced excitations or inhibitions of CA1 multiunit activity in the pOxr1/ArchT, Wfs1/ChR2, Wfs1/eArch, pOxr1/ChR2 anaesthetized mice. Lower panels: the averaged data of the firing frequency of CA1 pyramidal cells during light-OFF and light-ON periods (n=3 mice each group) **(C-D)** Time course of freezing observed in ArchT-expressing pOxr1-Cre mice and control mice in the TFC during training on day 1 (C) and testing on day 2 (D). Gray and green bars represent tone and shock, respectively. In the right panel of (D) and corresponding panels hereafter, freezing levels during the testing were averaged over the three 60-s tone periods and over the three first 60-s post-tone periods. **(E-H)** Time course of freezing observed in ChR2-eYFP-expressing, and eYFP only-expressing Wfs1-Cre mice in TFC (E-F) and DFC (G-H) during training on day 1 (E, G) and

testing on day 2 (F, H). In (G), blue light was delivered during training periods (22 s). (**I-J**) Blue light was delivered during tone periods (20 s) or trace+shock periods (22 s). Time courses of freezing observed in ChR2-expressing Wfs1-Cre mice in TFC during training on day 1 (I) or testing on day 2 (J). **(K-N)** Time course of freezing observed in eArch-eYFP expressing, and eYFP only-expressing Wfs1-Cre mice in TFC (K-L), and weak TFC (M-N) during training on day 1 (K, M) and testing on day 2 (L, N). In the right panels of (L) and (N) freezing levels during testing on day 2 averaged over the first, second and third 60-s post-tone periods. **(O-P)** Time course of freezing observed in ChR2mCherry expressing, and mCherry only-expressing pOxr1-Cre mice in weak TFC during training on day 1 (O) and testing on day 2 (P). *P<0.05.

References and Notes

1. E. Tulving, *Annu Rev Psychol* **53**, 1 (2002).
2. H. Eichenbaum, *Nat Rev Neurosci* **1**, 41 (Oct, 2000).
3. E. L. Hargreaves, G. Rao, I. Lee, J. J. Knierim, *Science* **308**, 1792 (Jun 17, 2005).
4. D. Marr, *Philos Trans R Soc Lond B Biol Sci* **262**, 23 (Jul 1, 1971).
5. K. Nakazawa *et al.*, *Science* **297**, 211 (Jul 12, 2002).
6. T. J. McHugh *et al.*, *Science* **317**, 94 (Jul 6, 2007).
7. G. V. Wallenstein, H. Eichenbaum, M. E. Hasselmo, *Trends Neurosci* **21**, 317 (Aug, 1998).
8. C. J. MacDonald, K. Q. Lepage, U. T. Eden, H. Eichenbaum, *Neuron* **71**, 737 (Aug 25, 2011).
9. J. Suh, A. J. Rivest, T. Nakashiba, T. Tominaga, S. Tonegawa, *Science* **334**, 1415 (Dec 9, 2011).
10. J. Kawano *et al.*, *Neurosci Res* **64**, 213 (Jun, 2009).
11. Y. Fujimaru, T. Kosaka, *Neurosci Res* **24**, 329 (Mar, 1996).
12. N. Tamamaki, Y. Nojyo, *Hippocampus* **3**, 471 (Oct, 1993).
13. J. J. Couey *et al.*, *Nat Neurosci* **16**, 318 (Mar, 2013).
14. C. Varga, S. Y. Lee, I. Soltesz, *Nat Neurosci* **13**, 822 (Jul, 2010).
15. A. Alonso, R. Klink, *J Neurophysiol* **70**, 128 (Jul, 1993).
16. R. Klink, A. Alonso, *Hippocampus* **7**, 571 (1997).
17. J. Mattis *et al.*, *Nat Methods* **9**, 159 (Feb, 2012).
18. S. E. Lee *et al.*, *Proc Natl Acad Sci U S A* **107**, 16994 (Sep 28, 2010).
19. A. Hjorth-Simonsen, J. Zimmer, *J Comp Neurol* **161**, 57 (May 1, 1975).
20. S. Zhao *et al.*, *Nat Methods* **8**, 745 (Sep, 2011).
21. T. F. Freund, G. Buzsaki, *Hippocampus* **6**, 347 (1996).
22. S. Bertrand, J. C. Lacaille, *J Physiol* **532**, 369 (Apr 15, 2001).
23. X. Han *et al.*, *Front Syst Neurosci* **5**, 18 (2011).
24. O. Yizhar, L. E. Fenno, T. J. Davidson, M. Mogri, K. Deisseroth, *Neuron* **71**, 9 (Jul 14, 2011).
25. J. S. Isaacson, M. Scanziani, *Neuron* **72**, 231 (Oct 20, 2011).
26. P. Andersen, R. Morris, D. Amaral, T. Bliss, J. O'Keefe, *The Hippocampus Book*. (2007).
27. R. F. Hevner, M. T. Wong-Riley, *J Comp Neurol* **326**, 451 (Dec 15, 1992).
28. A. Burgalossi *et al.*, *Neuron* **70**, 773 (May 26, 2011).
29. R. M. Empson, U. Heinemann, *J Physiol* **484 (Pt 3)**, 707 (May 1, 1995).
30. H. Dvorak-Carbone, E. M. Schuman, *J Neurophysiol* **82**, 3213 (Dec, 1999).
31. C. J. Price *et al.*, *J Neurosci* **25**, 6775 (Jul 20, 2005).
32. A. V. Egorov, B. N. Hamam, E. Fransen, M. E. Hasselmo, A. A. Alonso, *Nature* **420**, 173 (Nov 14, 2002).
33. T. T. Hahn, J. M. McFarland, S. Berberich, B. Sakmann, M. R. Mehta, *Nat Neurosci* **15**, 1531 (Nov, 2012).
34. O. P. Ottersen, *J Comp Neurol* **205**, 30 (Feb 10, 1982).
35. M. Fendt, M. S. Fanselow, *Neurosci Biobehav Rev* **23**, 743 (May, 1999).
36. S. Melzer *et al.*, *Science* **335**, 1506 (Mar 23, 2012).
37. M. Remondes, E. M. Schuman, *Nature* **416**, 736 (Apr 18, 2002).

Acknowledgments: We thank K. Deisseroth (ChR2 and eArch3.0 construct), and E. Boyden (ArchT construct) for providing the plasmids, R. Neve for generating the AAV-DIO-Synaptophysin-mCherry, J. Martin, C. Ragion, N. Nayyar, M. Serock, L. Sultzman, M. Ragion, L. Smith, A. Rivest for experimental help, J. Young, C. Yokoyama, T. Ryan, R. Redondo, X. Liu, K. Mulroy for comments, and the members of Tonegawa lab for support. This work was supported by the RIKEN Brain Science Institute.

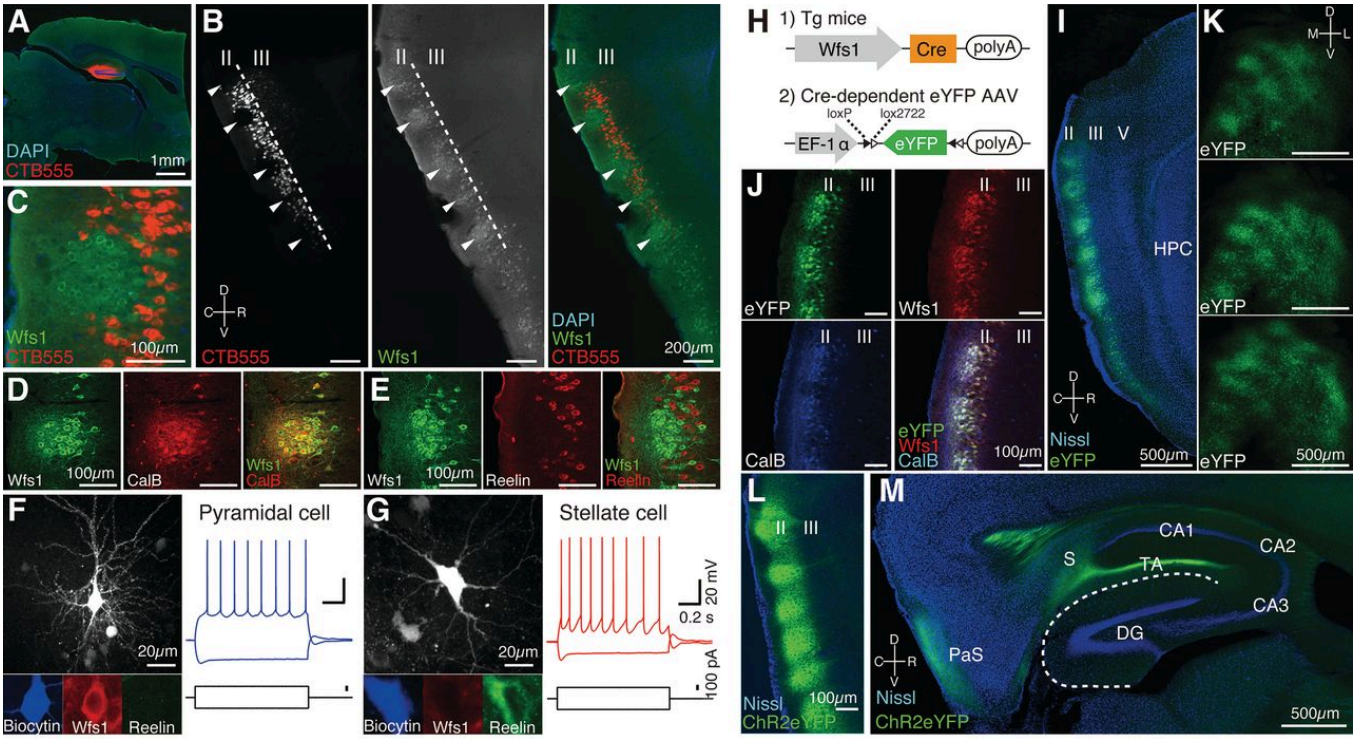
A
DAPI
CTB555
1mm
B
II III
CTB555
C
Wfs1
CTB555
100μm
Wfs1
DAPI
Wfs1
CTB555
200μm
D
Wfs1
100μm
CalB
Wfs1
CalB
E
Wfs1
100μm
Reelin
Wfs1
Reelin
F
20μm
Pyramidal cell
Biocytin
Wfs1
Reelin
G
20μm
Stellate cell
20 mV
0.2 s
100 pA
Biocytin
Wfs1
Reelin
H
1) Tg mice
Wfs1
Cre
polyA
2) Cre-dependent eYFP AAV
loxP
lox2722
EF-1 α
eYFP
polyA
I
II III V
HPC
Nissl
eYFP
500μm
J
eYFP
Wfs1
CalB
eYFP
Wfs1
CalB
100μm
K
eYFP
eYFP
eYFP
500μm
L
Nissl
ChR2eYFP
100μm
M
CA1
CA2
S
TA
CA3
DG
PaS
Nissl
ChR2eYFP
500μm
Figure 1

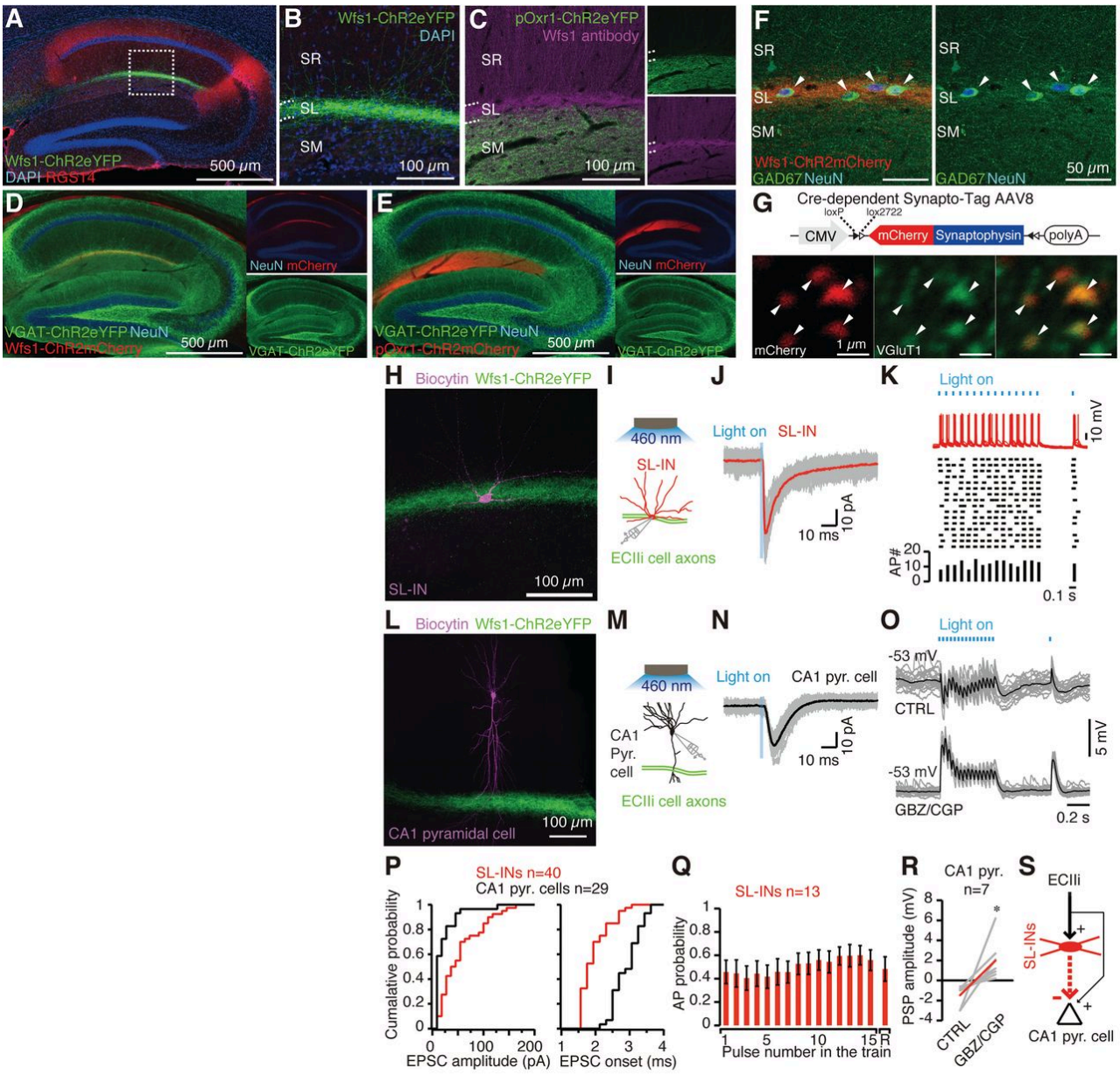
A
Wfs1-ChR2eYFP
DAPI RGS14
500 μm
B
Wfs1-ChR2eYFP
DAPI
SR
SL
SM
100 μm
C
pOxr1-ChR2eYFP
Wfs1 antibody
SR
SL
SM
100 μm
F
SR
SL
SM
Wfs1-ChR2mCherry
GAD67 NeuN
GAD67 NeuN
50 μm
D
NeuN mCherry
VGAT-ChR2eYFP NeuN
Wfs1-ChR2mCherry
500 μm
VGAT-ChR2eYFP
E
NeuN mCherry
VGAT-ChR2eYFP NeuN
pOxr1-ChR2mCherry
500 μm
VGAT-ChR2eYFP
G
Cre-dependent Synapto-Tag AAV8
loxP
lox2722
CMV
mCherry
Synaptophysin
polyA
mCherry
1 μm
VGluT1
H
Biocytin Wfs1-ChR2eYFP
SL-IN
100 μm
I
460 nm
SL-IN
ECIIi cell axons
J
Light on
SL-IN
10 pA
10 ms
K
Light on
10 mV
AP#
20
10
0
0.1 s
L
Biocytin Wfs1-ChR2eYFP
CA1 pyramidal cell
100 μm
M
460 nm
CA1
Pyr.
cell
ECIIi cell axons
N
Light on
CA1 pyr. cell
10 pA
10 ms
O
Light on
-53 mV
CTRL
-53 mV
GBZ/CGP
5 mV
0.2 s
P
SL-INs n=40
CA1 pyr. cells n=29
Cumulative probability
EPSC amplitude (pA)
EPSC onset (ms)
Q
SL-INs n=13
AP probability
Pulse number in the train
R
CA1 pyr.
n=7
PSP amplitude (mV)
CTRL
GBZ/CGP
S
ECIIi
SL-INs
CA1 pyr. cell

Figure 2

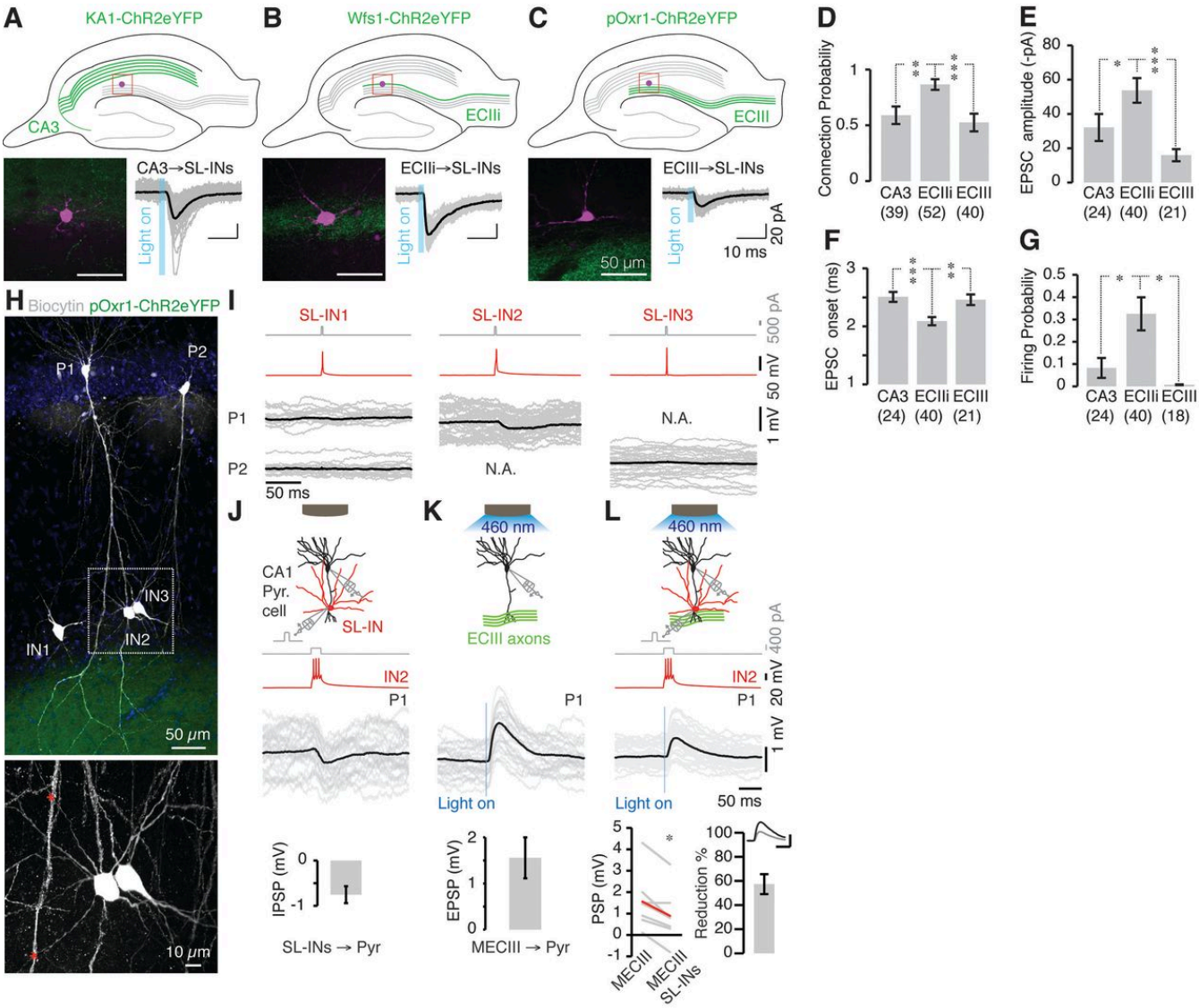
A
KA1-ChR2eYFP
CA3
CA3→SL-INs
Light on
B
Wfs1-ChR2eYFP
ECIIi
ECIIi→SL-INs
Light on
C
pOxr1-ChR2eYFP
ECIII
ECIII→SL-INs
Light on
50 µm
20 pA
10 ms
D
Connection Probability
CA3 (39)
ECIIi (52)
ECIII (40)
E
EPSC amplitude (-pA)
CA3 (24)
ECIIi (40)
ECIII (21)
F
EPSC onset (ms)
CA3 (24)
ECIIi (40)
ECIII (21)
G
Firing Probability
CA3 (24)
ECIIi (40)
ECIII (18)
H
Biocytin pOxr1-ChR2eYFP
P1
P2
IN1
IN2
IN3
50 µm
10 µm
I
SL-IN1
SL-IN2
SL-IN3
500 pA
50 mV
P1
P2
N.A.
1 mV
50 ms
J
CA1 Pyr. cell
SL-IN
IN2
P1
IPSP (mV)
SL-INs → Pyr
K
460 nm
ECIII axons
P1
Light on
EPSP (mV)
MECIII → Pyr
L
460 nm
IN2
P1
400 pA
20 mV
1 mV
Light on
50 ms
PSP (mV)
Reduction %
MECIII
MECIII
SL-INs

Figure 3

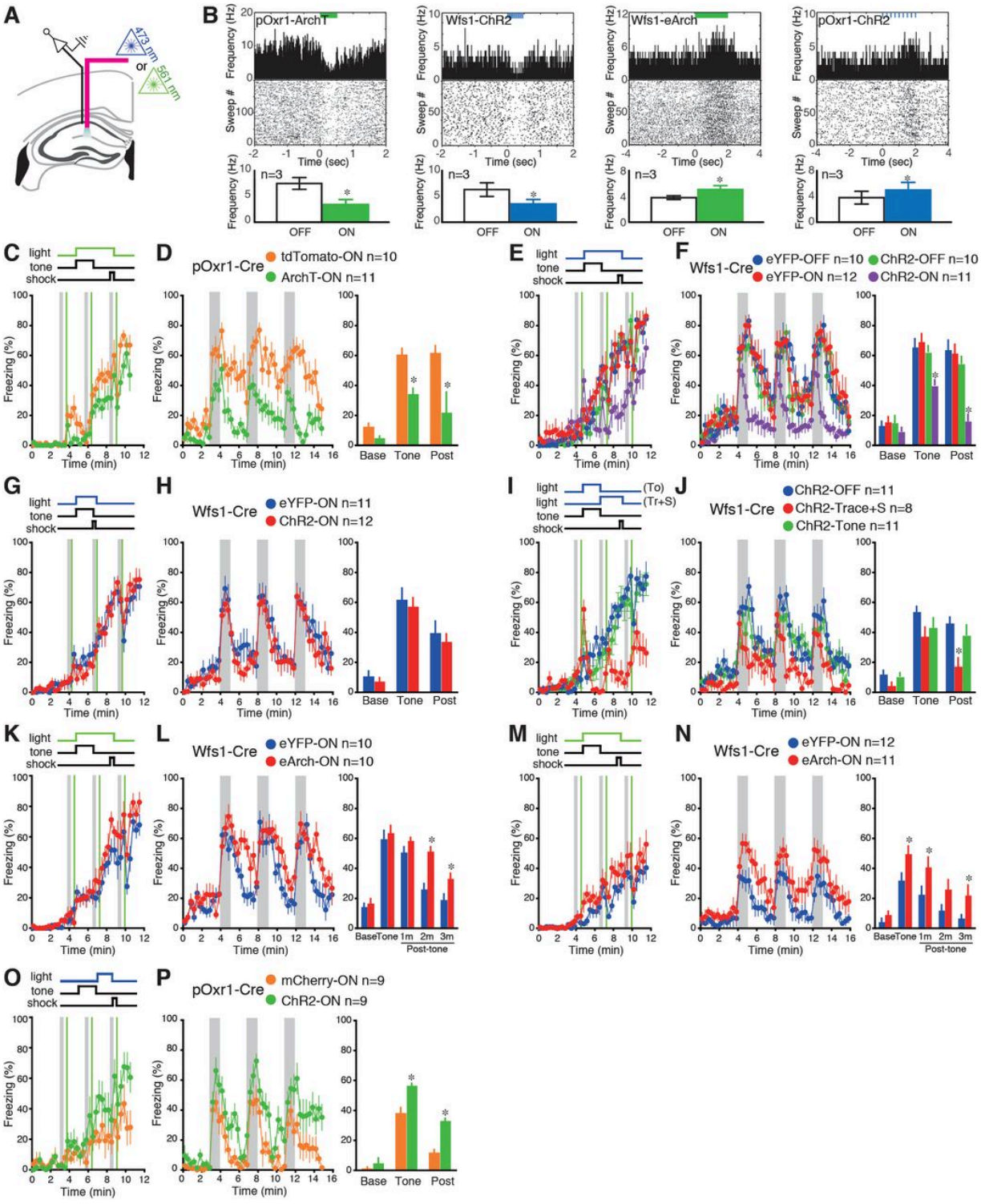
A
473 nm
or
561 nm
B
pOxr1-ArchT
Wfs1-ChR2
Wfs1-eArch
pOxr1-ChR2
Frequency (Hz)
Sweep #
Time (sec)
n=3
OFF
ON
C
light
tone
shock
Freezing (%)
Time (min)
D
pOxr1-Cre
tdTomato-ON n=10
ArchT-ON n=11
Base
Tone
Post
E
F
Wfs1-Cre
eYFP-OFF n=10
ChR2-OFF n=10
eYFP-ON n=12
ChR2-ON n=11
G
H
eYFP-ON n=11
ChR2-ON n=12
I
(To)
(Tr+S)
J
ChR2-OFF n=11
ChR2-Trace+S n=8
ChR2-Tone n=11
K
L
eYFP-ON n=10
eArch-ON n=10
BaseTone
1m
2m
3m
Post-tone
M
N
eYFP-ON n=12
eArch-ON n=11
O
P
mCherry-ON n=9
ChR2-ON n=9

Figure 4